TECHNICAL PROGRESS REPORT

A: COVER SHEET

Name of Submitting Organization: Nuonics, Inc.
Address of Submitting Organization: 1025 S. Semoran Blvd, Suite 1093, Winter Park, FL 32792
Tel/Fax: 407-379-0164

Name & Address of Sub-Contractor: University of Central Florida, 4000 Central Florida Blvd., CREOL Bldg, Orlando, FL 32816-2700

DOE Award No.: DE-FC26-03NT41923

Project Title: Ultra-High Temperature Sensors Based on Optical Property Modulation and Vibration-Tolerant Interferometry

Dated: May 21, 2007.

Principal Author: Dr. Nabeel A. Riza (email: nriza@aol.com)

Period Covered by Report: Oct 1, 2006 – March 31, 2007.
Type of Report: Semi-Annual Technical Progress Report

B: ABSTRACT

The goals of the this part of the Continuation Phase 2 period (Oct. 1, 06 to March 31, 07) of this project were to (a) fabricate laser-doped SiC wafers and start testing the SiC chips for individual gas species sensing under high temperature and pressure conditions and (b) demonstrate the designs and workings of a temperature probe suited for industrial power generation turbine environment. A focus of the reported work done via Kar UCF LAMP lab. is to fabricate the embedded optical phase or doped microstructures based SiC chips, namely, Chromium (C) , Boron (B) and Aluminium (Al) doped 4H-SiC, and to eventually deploy such laser-doped chips to enable gas species sensing under high temperature and pressure. Experimental data is provided from SiC chip optical response for various gas species such as pure N_2 and mixtures of N_2 and H_2, N_2 and CO, N_2 and CO_2, and N_2 and CH_4. Another main focus of the reported work was a temperature sensor probe assembly design and initial testing. The probe transmit-receive fiber-optics were designed and tested for electrically controlled alignment. This probe design was provided to overcome mechanical vibrations in typical industrial scenarios. All these goals have been achieved and are described in detail in the report.

C: TABLE OF CONTENTS

D: LIST OF GRAPHICAL MATERIALS

Fig. 1 Schematic diagram of the LAMP Lab. experimental setup for the gas sensing experiment.

Figure 2: Reflected power of silicon carbide upon exposure to nitrogen gas at different pressure (a) 296 psi and (b) 300 psi (c) 392 psi (d) 400 psi as a function of temperature from 20^{o}C upto 400^{o}C for normal incidence angle.

Figure 3: (a) (I) Reflected power of silicon carbide upon exposure to nitrogen and hydrogen partial gas pressure: Nitrogen 294 psi + Hydrogen 4 psi as a function of temperature from 20^{o}C upto 400^{o}C for normal incidence angle. (II) Contribution of hydrogen on the refractive index of compressed layer at total pressure of 300 psi as a function of temperature from 20^{o}C upto 400^{o}C. (b) (I) Reflected power of silicon carbide upon exposure to nitrogen and hydrogen partial as pressure: Nitrogen 392 psi + Hydrogen 8 psi as a function of temperature from 20^{o}C upto 400^{o}C for normal incidence angle. (II) Contribution of hydrogen on the refractive index of compressed layer at total pressure of 400 psi as a function of temperature from 20^{o}C upto 400^{o}C.

Figure 4: (a) (I) Reflected power of silicon carbide upon exposure to nitrogen and carbon monoxide partial gas pressure: Nitrogen 294 psi + Carbon Monoxide 4 psi as a function of temperature from 20^{o}C upto 400^{o}C for normal incidence angle. (II) Contribution of carbon monoxide on the refractive index of compressed layer at total pressure of 300 psi as a function of temperature from 20^{o}C upto 400^{o}C. (b) (I) Reflected power of silicon carbide upon exposure to nitrogen and carbon monoxide as pressure: Nitrogen 392 psi + Carbon Monoxide 8 psi as a function of temperature from 20^{o}C upto 400^{o}C for normal incidence angle. (II) Contribution of

carbon monoxide on the refractive index of compressed layer at total pressure of 400 psi as a function of temperature from 20^{o}C upto 400^{o}C.

Figure 5: (a) (I) Reflected power of silicon carbide upon exposure to nitrogen and carbon dioxide partial gas pressure: Nitrogen 294 psi + Carbon Dioxide 4 psi as a function of temperature from 20^{o}C upto 400^{o}C for normal incidence angle. (II) Contribution of carbon dioxide on the refractive index of compressed layer at total pressure of 300 psi as a function of temperature from 20^{o}C upto 400^{o}C. (b) (I) Reflected power of silicon carbide upon exposure to nitrogen and carbon dioxide as pressure: Nitrogen 392 psi + Carbon Dioxide 8 psi as a function of temperature from 20^{o}C upto 400^{o}C for normal incidence angle. (II) Contribution of carbon dioxide on the refractive index of compressed layer at total pressure of 400 psi as a function of temperature from 20^{o}C upto 400^{o}C.

Figure 6: (a) (I) Reflected power of silicon carbide upon exposure to nitrogen and methane partial gas pressure: Nitrogen 294 psi + Methane 4 psi as a function of temperature from 20^{o}C upto 400^{o}C for normal incidence angle. (II) Contribution of methane on the refractive index of compressed layer at total pressure of 300 psi as a function of temperature from 20^{o}C upto 400^{o}C.

Figure 7: Contribution of different gas species on refractive index of the compressed layer at a partial pressure of 4 psi as a function of temperature from 20^{o}C upto 400^{o}C. (Calculated from experimental data)

Figure 8: Contribution of different gas species on refractive index of the compressed layer at a partial pressure of 8 psi as a function of temperature from 20^{o}C upto 400^{o}C. (Calculated from experimental data)

Figure 9a. Boron-doped 4H- SiC (n type).

Figure 9b. Aluminum-doped 4H- SiC (n type).

Figure 9c. Chromium-doped 4H- SiC (n type).

Figure 10. Project activities for SiC chip development, sensor fabrication and optical response studies.

Fig. 11: Proposed Extreme Temperature Hybrid Design Optical Sensor using SiC sensing and packaging technology. PD: Photo-Detector; TL: Tunable Laser; SMF: Single Mode Fiber.

Fig.12 Example High Pressure High Temperature Seal SiC Tube that forms the basis of the SiC chip front-end packaging.

Fig. 13: Fabricated Laser Beam Smart Transceiver Module using Electronically Controlled Beam Alignment Mechanics.

Fig. 14: Automatic system alignment scenario in case of movement of SiC chip in probe within hot gas chamber.

Fig. 15. Laser beam from the transceiver module in various positions on a screen.

Nomenclature:

n_3 refractive index of composite layer

T_0 initial temperature (room temperature) of the sample

T_{Final} observation temperature

P_0 initial pressure (atmospheric pressure)

P_{Final} observation pressure

E elastic modulus of the sample

α linear thermal expansion coefficient of the sample

λ_0 wavelength of light in vacuum

d_0 initial thickness of the sample

E: INTRODUCTION

The purpose of this project is to develop a science and engineering base to develop sensors for ultra high temperature fossil fuel applications. The sensors proposed are based on the principle of the Optical Path Length (OPL) variation in a medium owing to the dependence of the optical property (e.g., refractive index) of a high temperature material, such as silicon carbide (SiC), on the temperature, pressure, or species concentration. By use of special design optics and signal processing in combination with remotely located SiC frontend chips, one could design optical sensors of measuring temperature, pressure, and gas species, as investigated in this project. Note that the leading fiber-optic sensors require costly environmental protection of the light delivery and light return fiber. This is because the fiber intrinsically contains both the sensing zone that must react to the changing environmental conditions (e.g., temperature) and the light delivery fiber that should stay protected and essentially unaffected from changing environmental effects. It is well known that standard low loss single mode optical fibers (SMFs) are made of glass, with transition temperatures around 475 °C, leading to unwanted softening of glass at higher temperatures. Thus, there exists a dilemma for the sensor design engineer using the mentioned fiber-optic sensors. In the proposed hybrid sensor design, this dilemma is removed as a fiber takes light to the safe point and then a free-space laser beam reads sensing parameters off the SiC chip in the hot zone, thus producing no physical contact between the harsh environment and the light delivery and processing optics. In effect, one can imagine many low cost SiC optical chips distributed in the desired sensing zone where a scanning free-space laser beam rapidly engages these sensor frontend chips to produce signals for later data processing and environmental parameter recovery. In effect, a truly non-invasive distributed optical sensor is realized.

F: EXECUTIVE SUMMARY

Accomplishments during this phase of the project have been achieved on two fronts, namely; (a) Fabrication of Doped SiC chips and initial testing of SiC chip for enabling gas species sensing at high temperatures and pressures and (b) Initial temperature probe assembly design, assembly, and testing to enable industrial deployment.

The first primary objective was achieved by fabricating different SiC doped chip samples, i.e., (1) Chromium (C) doped 4H-SiC (2) Boron (B) doped 4H-SiC and (3) Aluminium (Al) doped 4H-SiC. Another objective was to use a 4H-SiC chip's measured reflected interference patterns and calculate the refractive indices of combustion gases such as nitrogen (N_2), carbon monoxide (CO), carbon dioxide (CO_2), methane (CH_4) at different temperatures and pressures. Initial experiments have been conducted for pure N_2 and mixtures of N_2 and H_2, N_2 and CO, N_2 and CO_2, and N_2 and CH_4. The resulting interference patterns of the reflected power from the SiC chip has been analyzed.

The second objective was achieved by engaging with Siemens, a major power generation systems design house, to access probe mechanical design requirements to handle the extreme temperature and high pressures of the Siemens power plant rig. Specifically, a vibration tolerant Transmit-Receive (T-R) fiber-optics design of the probe assembly is currently under fabrication, assembly, and testing. Initial design, alignment and tracking experiments have been conducted.

G: EXPERIMENTAL RESULTS

G.1 SiC Chip-based Gas Species Optical Sensing at High Temperatures and Pressure (Kar LAMP Lab. Provided Data and Information):

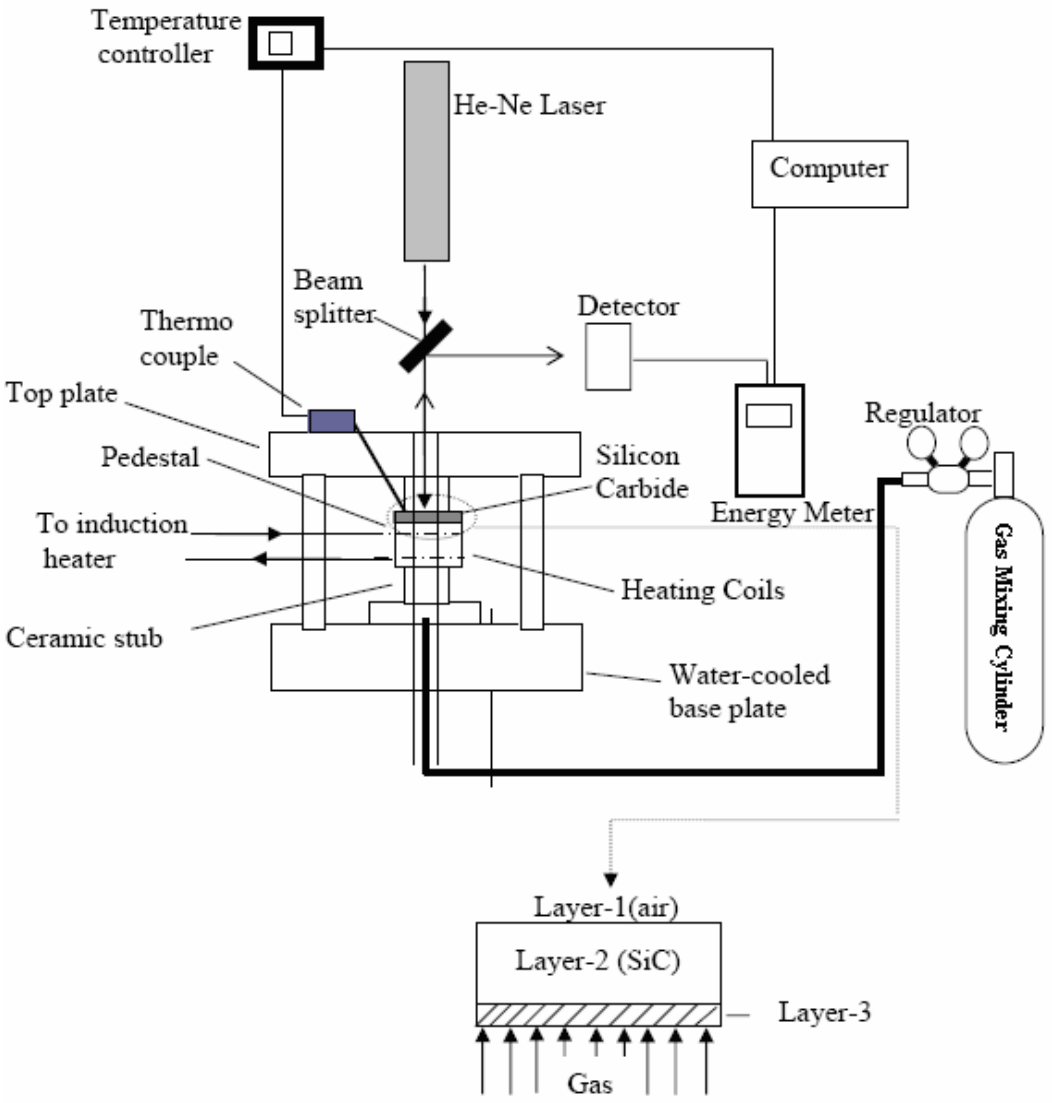

Fig. 1 Schematic diagram of the LAMP Lab. experimental setup for the gas sensing experiment.

In the Kar LAMP Lab., a continuous wave helium-neon (He-Ne) laser of wavelength 632.8 nm was used to understand the changes in the refractive index (n_3) of a compressed layer (see Fig. 1) at the chip-gas interface in the presence of a combustion gas such as H_2, CO, CO_2,

and CH_4 for the laser doped samples. The combustion gases are present in the combustor in trace amounts as presented in Table 1. The SiC chip is inherently a Fabry-Pérot interferometer enabling optical measurements pertaining to interference patterns that were analyzed to calculate the compressed layer refractive index, n_3.

"In 1995, ISE (Iniziative Sviluppo Energia) started construction of a new 'clean' power plant, called CET3, at ILVA Taranto, Italy. The plant consisted of three identical combined cycle units capable of producing 530 MW of electrical power. The plant was designed to utilize Blast Furnace Gas (BFG) and Linz Durer Gas (LDG). Dejong Coen was contracted to design and provide the supplementary firing system to produce steam at 540^{o}C. The burners were to utilize BFG and LDG gas supported by natural gas" [1]. The gas composition of the gas mixture for our case has been determined by the following BFG standard [1] as shown in Table 1.

Table 1. Typical combustion gas compositions.

Gas Type	BFG (Blast Furnace Gas) [mole %]	LDG (Linz Durer Gas) [mole %]
H_2	4.53	0.96
CH_4	<0.003	-
CO	22.38	69.15
CO_2	23.19	23.19
N_2	48.60	14.89
O_2	0.25	-

A single crystal 4H-SiC wafer of thickness 399 μm was used as an optical chip in this experiment. The experimental setup for studying the optical properties of the chip is shown in Fig. 1. The chip was heated using a steel pedestal as shown in Fig. 1 and the bottom surface of the chip was exposed to the gas mixtures at different pressures. Due to high thermal conductivity of SiC, the thermal energy is transferred to the gas mixture at the chip-gas interface,

creating a thermal boundary layer containing hot gas mixture at the interface. This enables us to test the sensing capability of SiC at high temperatures, pressures and gas species. The effects of the pressure, temperature, and gas compositions of H_2, CO, CO_2, and CH_4 on the optical response of the 4H-SiC chip have been studied by examining the reflectivity of the chip. The SiC chip serves as an amplitude-splitting device, so that two reflected lights may be considered as arising from two coherent virtual sources lying behind the silicon carbide wafer. This optical property of SiC makes it an interferometric sensor inherently, enabling highly sensitive remote sensing. A compressed layer (Fig. 1), which consists of compressed SiC atomic layers and hot gases at the chip-gas interface, is formed at the interface due to high pressures and temperatures of the gas mixture. The interface of SiC experiences compressive stresses under high gas pressures and this produces a denser atomic layer of SiC near its bottom surface than the rest of the upper region of the chip.

The measured reflected power exhibits interference pattern with alternating maximum and minimum powers generated by constructive and destructive interference of light respectively for different gas compositions as shown in Fig. 2 for pure nitrogen, 3a (I) and 3b (I) for nitrogen-hydrogen mixture, 4a(I) and 4b(I) for nitrogen-carbon monoxide mixture, 5a(I) and 5b(I) for nitrogen-carbon dioxide mixture, 6a(I) for nitrogen-methane mixture. The patterns of the oscillations are unique to the type of gases. These patterns can be attributed to the characteristic identity of the individual gases in chemical sensing applications. The chip response is selective to the gas species. The refractive index of the composite layer changes depending on the gas species as shown in Fig. 3a (II) and 3b (II) for nitrogen-hydrogen mixture, 4a(II) and 4b(II) for nitrogen-carbon monoxide mixture, 5a(II) and 5b(II) for nitrogen-carbon dioxide mixture, 6a(II) for nitrogen-methane mixture.

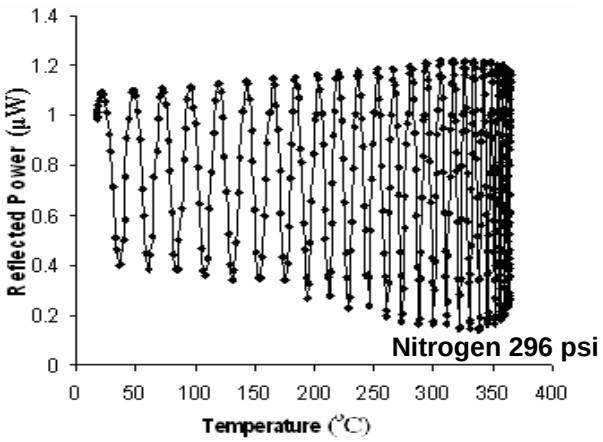

(a)

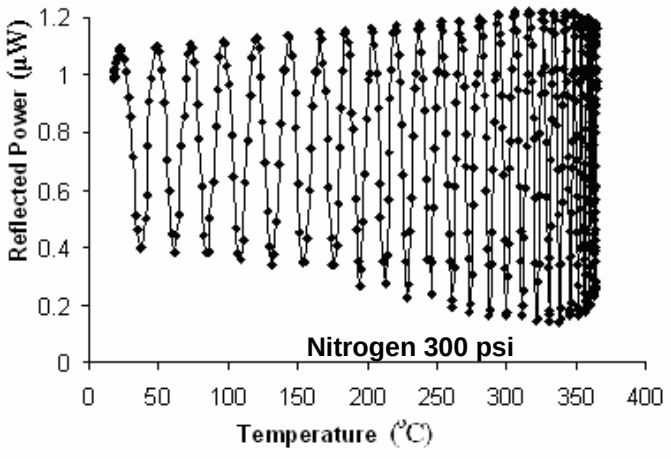

(b)

(c)

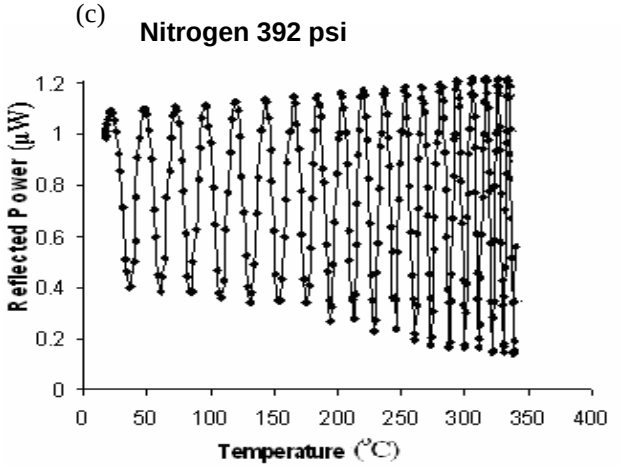

(d)

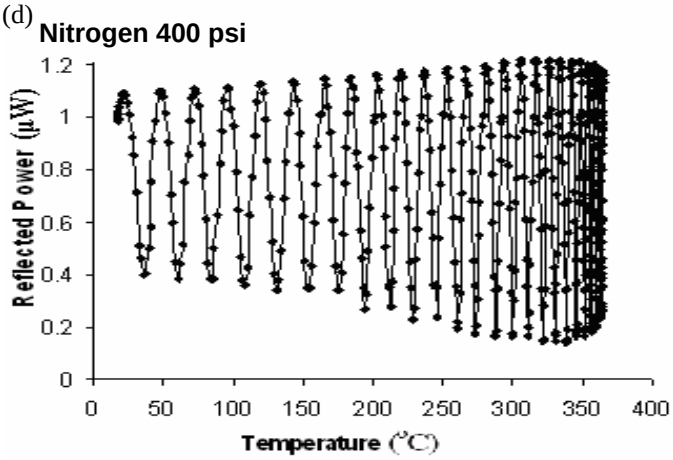

Fig. 2 Reflected power of silicon carbide upon exposure to nitrogen gas at Different pressure (a) 296 psi and (b) 300 psi (c) 392 psi (d) 400 psi as a function of temperature for normal incidence angle.

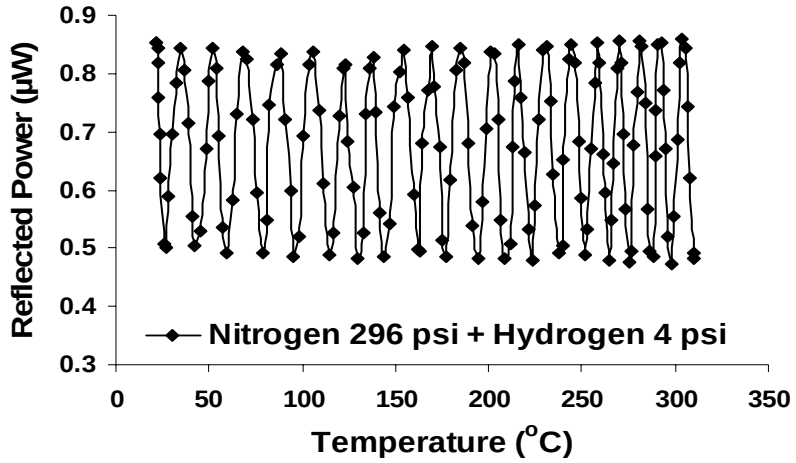

(I)

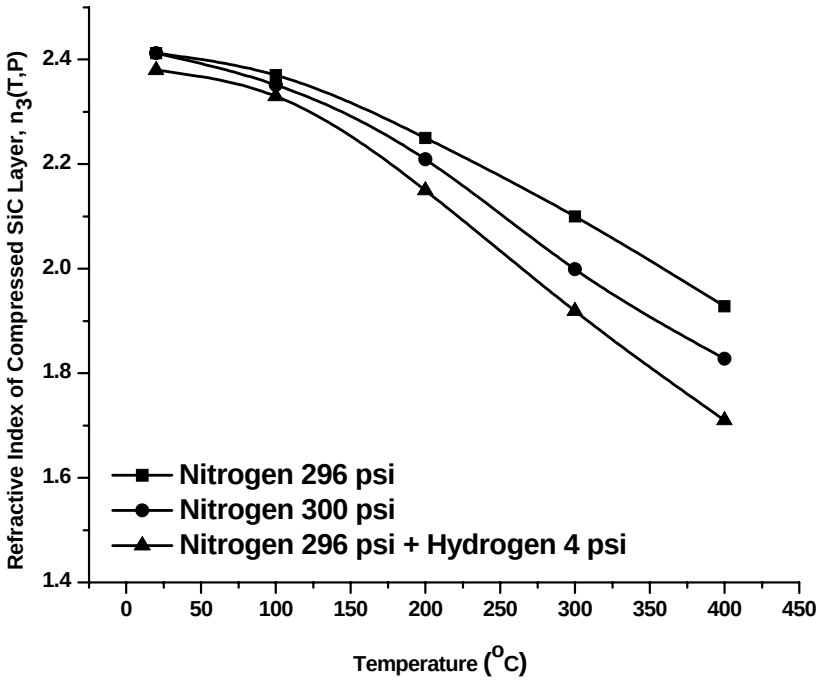

(II)

Fig. 3 (a) (I) Reflected power of silicon carbide upon exposure to nitrogen and Hydrogen partial gas pressure: Nitrogen 294 psi + Hydrogen 4 psi as a function of temperature for normal incidence angle. (II) Contribution of Hydrogen on the refractive index of compressed layer at total pressure of 300 psi as a function of temperature.

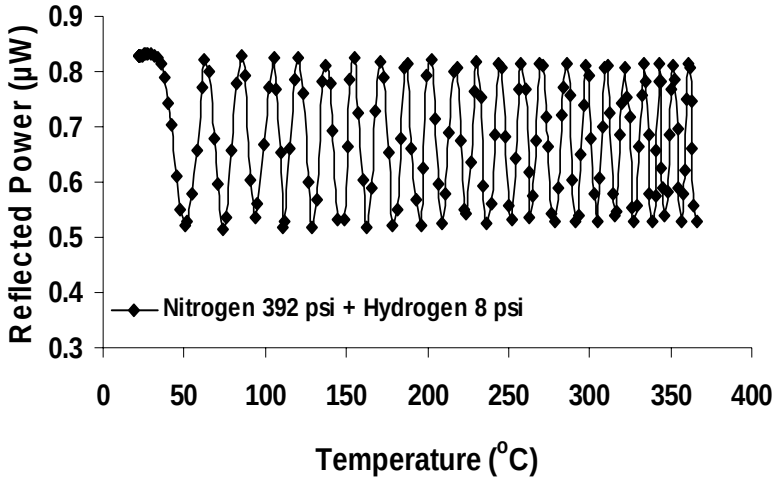

(I)

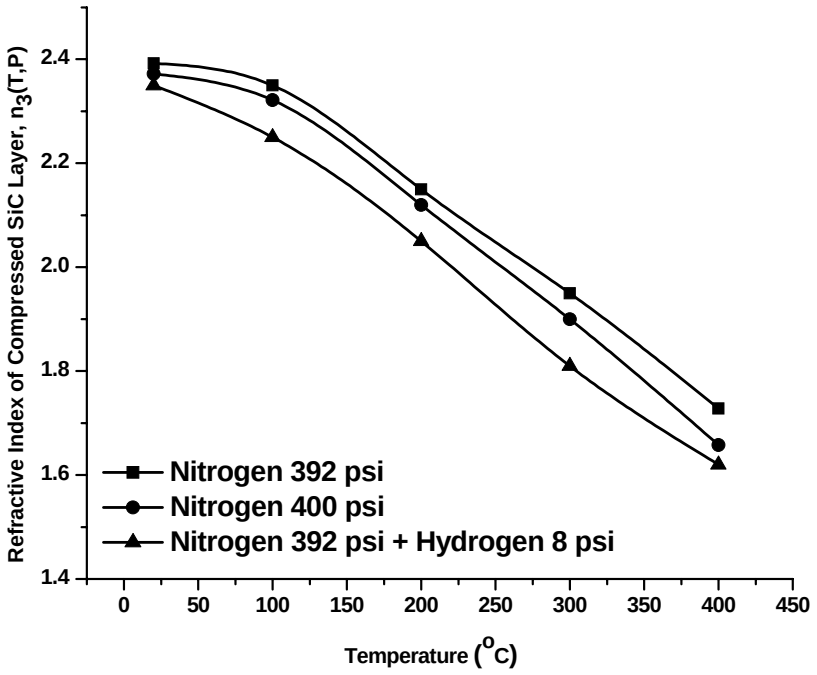

(II)

Fig. 3b (I) Reflected power of silicon carbide upon exposure to nitrogen and Hydrogen partial gas pressure: Nitrogen 392 psi + Hydrogen 8 psi as a function of temperature for normal incidence angle. (II) Contribution of Hydrogen on the refractive index of compressed layer at total pressure of 400 psi as a function of temperature.

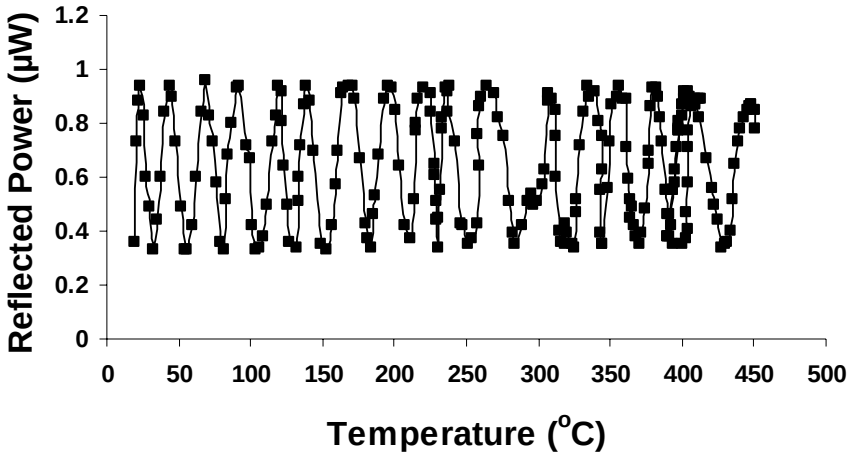

(I)

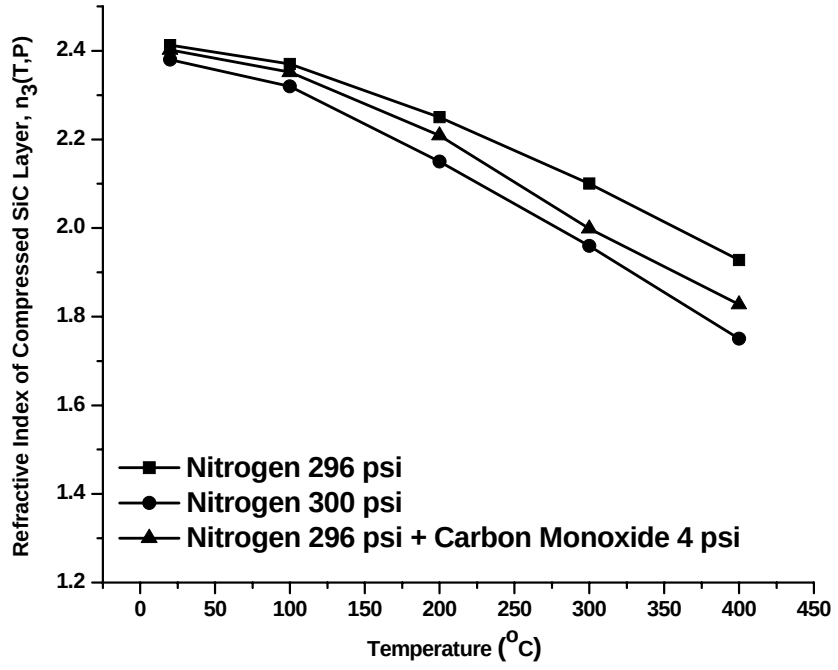

(II)

Fig. 4a (I) Reflected power of silicon carbide upon exposure to nitrogen and Carbon Monoxide partial gas pressure: Nitrogen 294 psi + Carbon Monoxide 4 psi as a function of temperature for normal incidence angle. (II) Contribution of Carbon Monoxide on the refractive index of compressed layer at total pressure of 300 psi as a function of temperature.

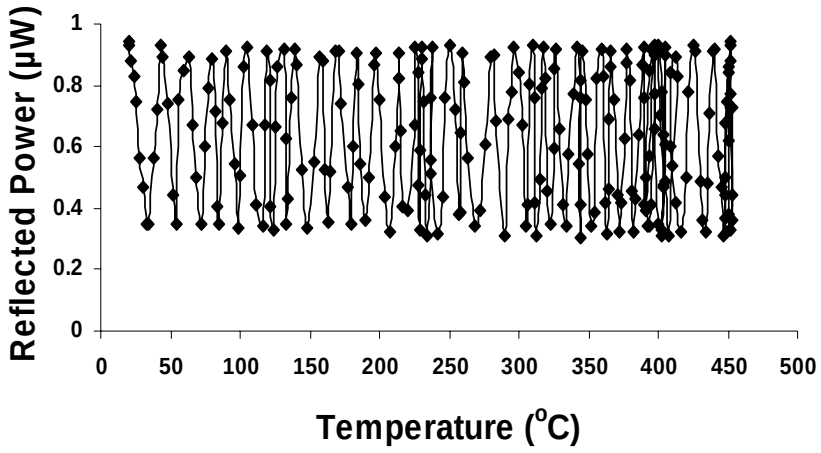

(I)

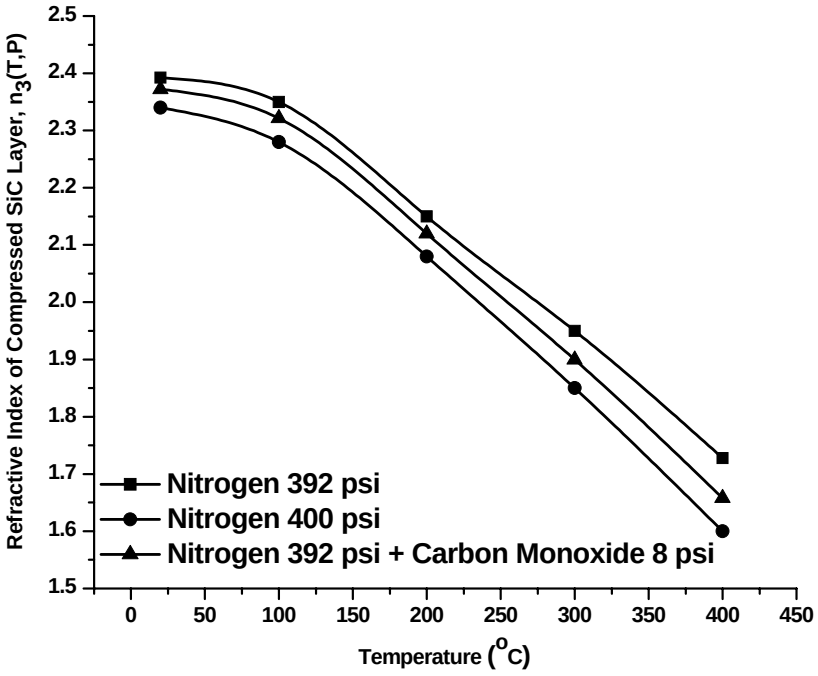

(II)

Fig. 4b (I) Reflected power of silicon carbide upon exposure to nitrogen and Carbon Monoxide partial gas pressure: Nitrogen 392 psi + Carbon Monoxide 8 psi as a function of temperature for normal incidence angle. (II) Contribution of Carbon Monoxide on the refractive index of compressed layer at total pressure of 400 psi as a function of temperature.

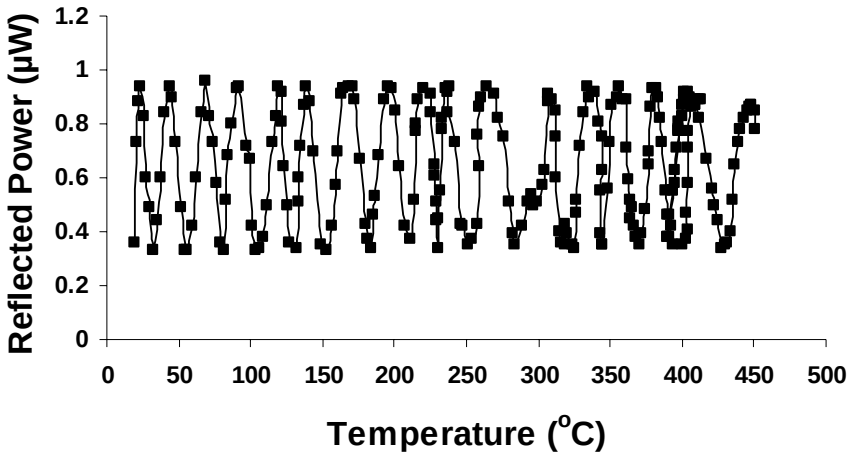

(I)

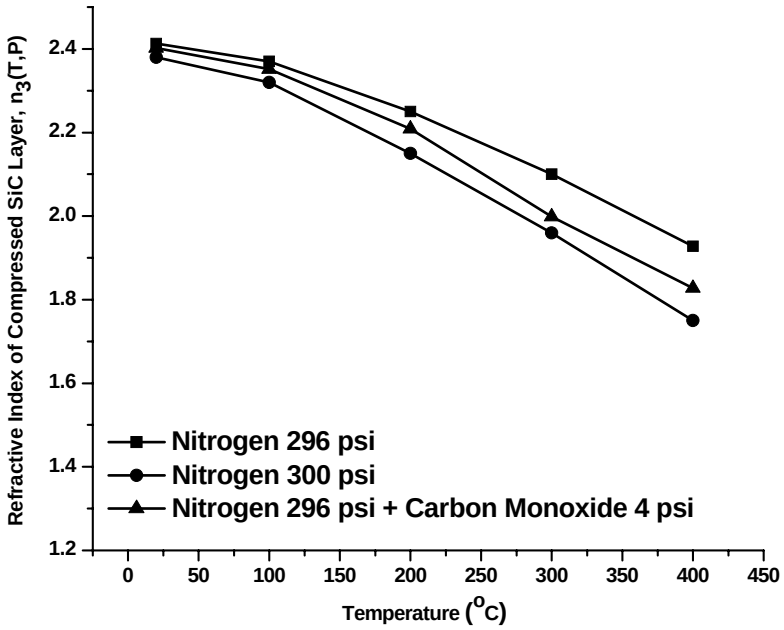

(II)

Fig. 5a(I) Reflected power of silicon carbide upon exposure to nitrogen and Carbon Monoxide partial gas pressure: Nitrogen 294 psi + Carbon Monoxide 4 psi as a function of temperature for normal incidence angle. (II) Contribution of Carbon Monoxide on the refractive index of compressed layer at total pressure of 300 psi as a function of temperature.

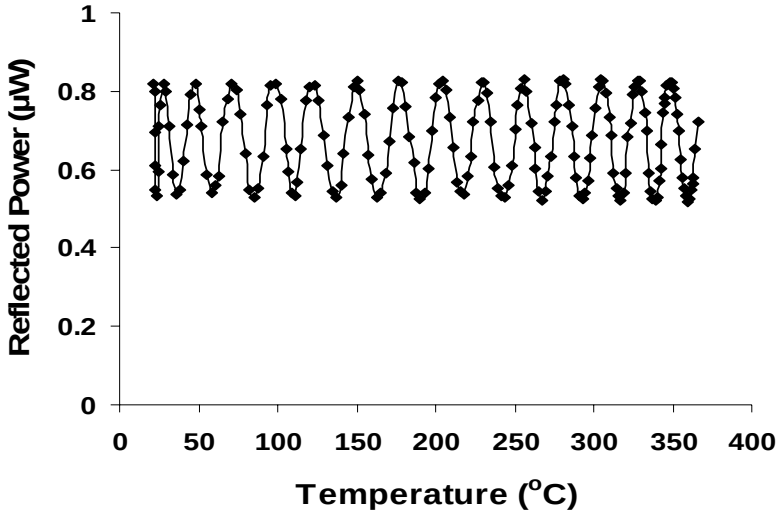

(I)

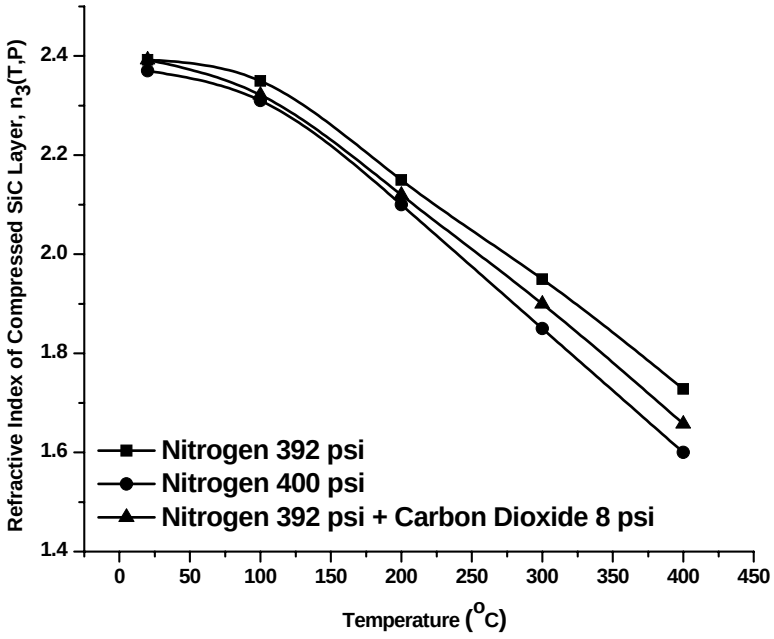

(II)

Fig. 5b (I) Reflected power of silicon carbide upon exposure to nitrogen and Carbon Dioxide partial gas pressure: Nitrogen 392 psi + Carbon Dioxide 8 psi as a function of temperature for normal incidence angle. (II) Contribution of Carbon Dioxide on the refractive index of compressed layer at total pressure of 400 psi as a function of temperature.

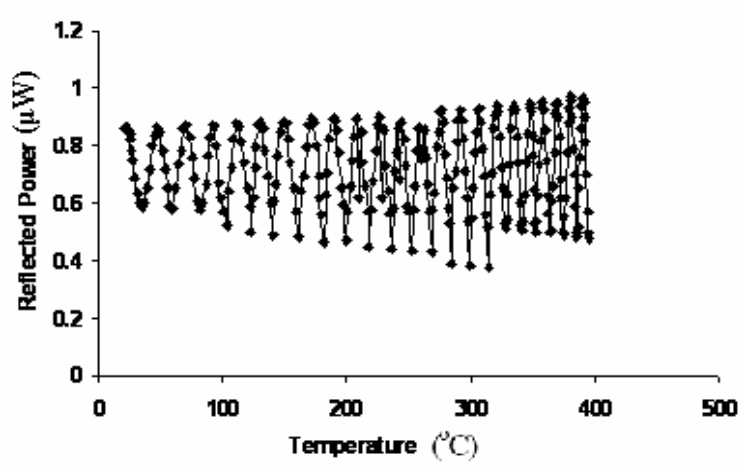

(I)

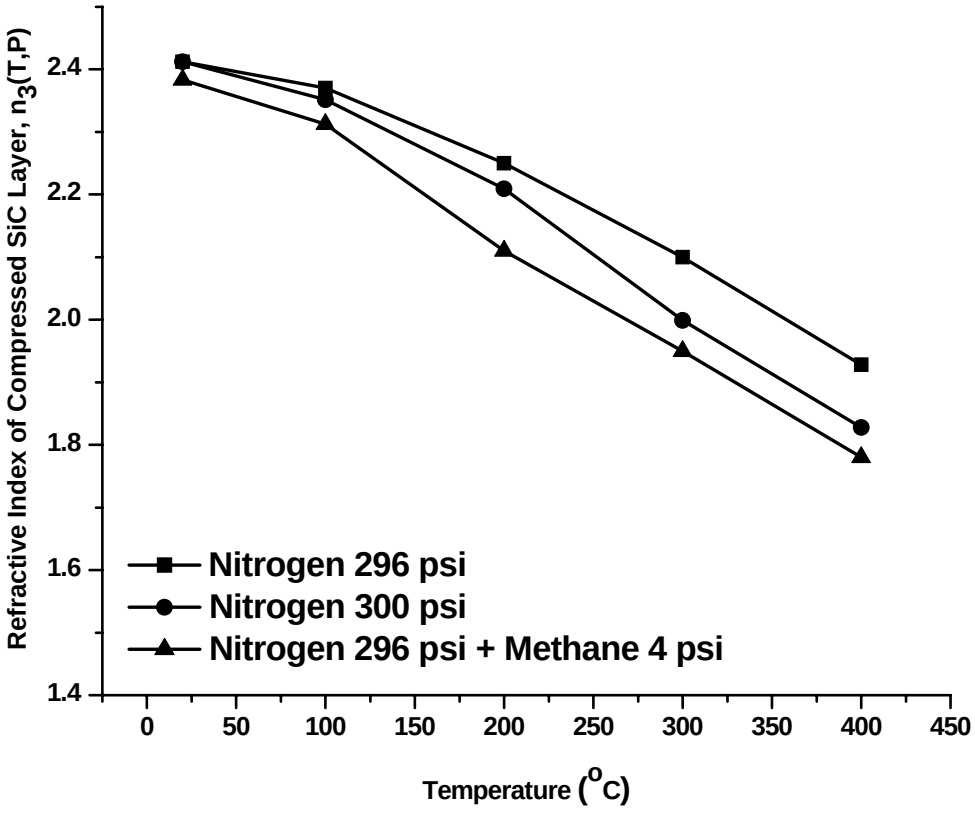

(II)

Fig. 6a (I) Reflected power of silicon carbide upon exposure to nitrogen and Methane partial gas pressure: Nitrogen 296 psi + Methane 4 psi as a function of temperature for normal incidence angle. (II) Contribution of Methane on the refractive index of compressed layer at total pressure of 300 psi as a function of temperature.

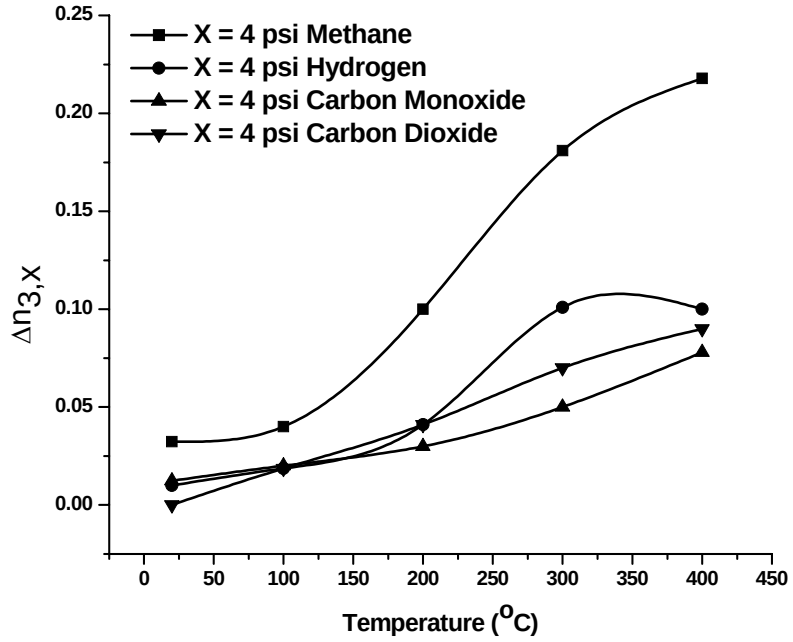

Fig. 7 Contribution of different gas species on refractive index of the compressed layer at a partial pressure of 4 psi as a function of temperature. (Calculated from experimental data)

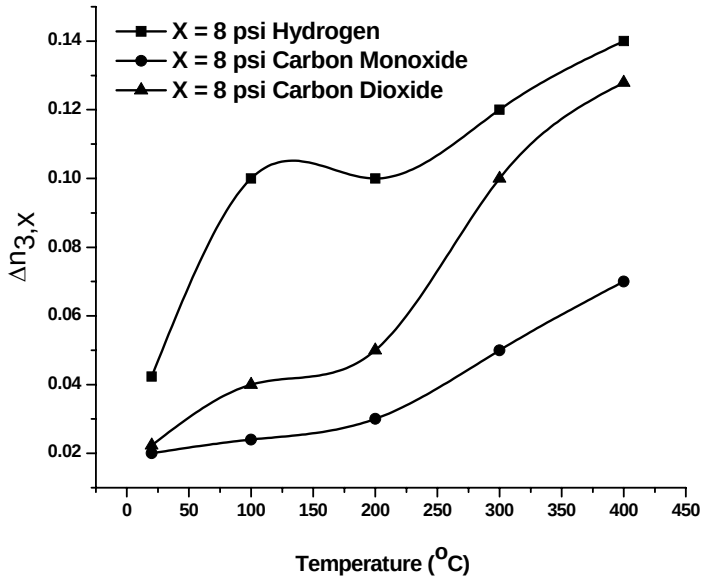

Fig. 8 Contribution of different gas species on refractive index of the compressed layer at a partial pressure of 8 psi as a function of temperature. (Calculated from experimental data)

The refractive index can be extracted from the interference pattern using the following expression [2-4]:

$$n_{m+1} = \frac{\lambda_0 + n_m d_0 \left[2 - \frac{1}{E}(\Delta P) - \alpha_{mid}(\Delta T) \right]}{d_0 \left[2 - \frac{3}{E}(\Delta P) + \alpha_{mid}(\Delta T) \right]} \quad (1)$$

Here $\Delta T = T_{Final1} - T_0$, $\Delta P = P_{Final} - P_0$. Various symbols in Eq. (1) are defined in the nomenclature section. From the refractive indices data, it is clearly observed that at high temperature and pressure the compressed layer refractive index decreases. Next described is the contribution ($\Delta n_{3,X}$) to the compressed layer refractive index due to different combustion gases. 'X' refers to different combustion gases such as H_2, CO, CO_2 and CH_4. The refractive index data can be used to sense all the different combustion gases. Let us say that the refractive index of the compressed layer is $n_{3,296N2}$ for 296 psi of nitrogen. When 4 psi of hydrogen added to 296 psi of pure nitrogen, the refractive index of the compressed layer due to this 300 psi gas mixture is $n_{3,296N2+4H2}$. The value of $n_{3,296N2+4H2}$ is less the value of $n_{3,296N2}$, indicating that 4 psi of hydrogen has reduced the compressed layer refractive index compare to the compressed layer refractive index in presence of 296 psi of pure nitrogen. This reduction in the compressed layer refractive index is given by,

$$\Delta n_{3,H2} = n_{3,296N2} - n_{3,296N2+4H2} \quad (2)$$

The reduction of compressed layer refractive index increases with temperature as shown in as shown in Fig. 3a (II) and 3b (II) for nitrogen-hydrogen mixture, 4a(II) and 4b(II) for nitrogen-carbon monoxide mixture, 5a(II) and 5b(II) for nitrogen-carbon dioxide mixture, 6a(II) for nitrogen-methane mixture.

In this section, the Kar LAMP Lab. discusses the change in compressed layer refractive index due to different combustion gas species mixtures compare to the same pressure of pure nitrogen. According to the earlier stated figures, it is clear that the compressed layer refractive indices of pure nitrogen pressure of 300 psi and the partial pressure of combustion gases with nitrogen of same pressure have distinct different value which indicates that the difference is due to the combustion gas species. It has been observed that for hydrogen partial pressure of 4 psi and 8 psi, the compressed layer refractive indices are less compare to the pure nitrogen pressure of 300 psi and 400 psi respectively. But for other combustion gases, the compressed layer refractive indices are larger than the pure nitrogen. So, the refractive indices data can be used to detect different combustion gas species.

Table 2: Contribution on compressed layer refractive index by different gas species.

Gas Species	Partial Pressure	Contribution $(\Delta n_{3,X})$ of combustion gases to the compressed layer $* \Delta n_{3,X} = n_{3,YN2} - n_{3,aN2+bX}$				
		20°C	100°C	200°C	300°C	400°C
H_2	4 psi	0.03	0.04	0.10	0.18	0.21
	8 psi	0.04	0.10	0.10	0.14	0.14
CO	4 psi	0.01	0.01	0.04	0.10	0.10
	8 psi	0.02	0.02	0.03	0.05	0.07
CO_2	4 psi	0.01	0.02	0.03	0.05	0.08
	8 psi	0.02	0.04	0.05	0.10	0.12
†CH_4	4 psi	0.01	0.02	0.04	0.10	0.10
	8 psi	-----	------	------	------	------

† Data for CH_4 at 8 psi is not present because our ceramic tube used for placing the sample holder broke. We have placed order for the ceramic tube and will include the data for this case in our next report.

* 'a' refers to the pressure of N_2 in the gas mixture, 'b' refers to the pressure of X (X= H_2, CO, CO_2, or CH_4) in the gas mixture, Y refers to the pressure of pure N_2 where Y= a, Y=296 psi when b=4 psi and Y= 392 psi when b = 8 psi.

The contribution of different combustion gases to the compressed layer refractive index have been tabulated in Table 2 and Figs. 7 and 8 are the graphical representation of the contributions. The presentation of Kar LAMP Lab. results in different figures for different total pressures of pure N_2 and partial pressures of different combustion gases are tabulated in Table 3.

Table 3: Figure numbers for different types of gases at different pressures.

	Pure N_2 [psi]				**N_2 + H_2 [psi]**		**N_2 + CO [psi]**		**N_2 + CO_2 [psi]**		**N_2 + CH_4 [psi]**	
	296	**300**	**392**	**400**	**296+4**	**392+8**	**296+4**	**392+8**	**296+4**	**392+8**	**296+4**	**392+8**
Fig. No. for reflected power	**2a**	**2b**	**2c**	**2d**	**3a(I)**	**3b(I)**	**4a(I)**	**4b(I)**	**5a(I)**	**5b(I)**	**6a(I)**	**6b(I)**
Fig. No. for n_3 of compressed layer					**3a(II)**	**3b(II)**	**4a(II)**	**4b(II)**	**5a(II)**	**5b(II)**	**6a(II)**	**6b(II)**

SiC Chip Doping Studies (Kar LAMP Lab. and AppliCote Associates Data):

All 6H-SiC parent wafers have been fabricated. Sample set (B and Cr doped) has been delivered. These wafers have been diced to a square shape with perfect dimension so that the sensor can fit into Kar's experimental setup with maximum gas sealing for experiments at high temperatures and high pressures using existing diamond saw technology. A very sharp diamond

saw blade was used to scribe a 1 cm × 1 cm grid in the wafer. A scribed corner or edge of the wafer was placed on a rectangular metal substrate aligning the scribe lines with the metal substrate edges; light tapping on the scribe lines freed the chips. This approach has proved adequate for our limited sample requirements. Digital pictures of the 1 cm × 1 cm SiC wafers are presented in Figs. 9a – c. Three doped chips were created by doping each of the wafers with a particular dopant such as B, Al or Cr. A laser doping technique that was developed at UCF for compound semiconductors, such as SiC, was used to fabricate doped chips. Various laser parameters used for the doping experiments are presented in Table 4.

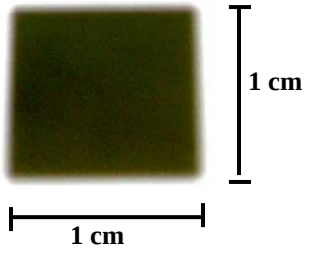

Fig. 9a. Boron-doped 4H- SiC (n type).

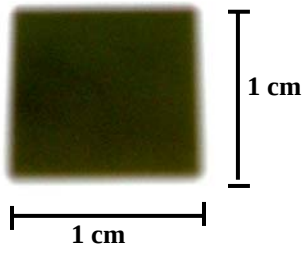

Fig. 9b. Aluminum-doped 4H- SiC (n type).

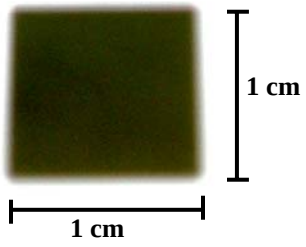

Fig. 9c. Chromium-doped 4H- SiC (n type).

AppliCote Associates (AA), LLC has completed modification of a scanning electron microscope coupled with energy dispersive spectra chemical analysis (SEM/EDS) sample stage, increasing its sample capacity. This approach was taken to economize materials characterization analysis and to allow “same time” evaluation of a group of samples to better understand inconsistencies and trends in processing. Analysis of the samples showed no surface damage or defect generation; the requirement for iteration is unlikely. These cyclic activities are illustrated in Fig. 10.

Table 4: Parameters used for laser doping of silicon carbide to fabricate combustion gas chips.

Doping conditions	Fig. 1a (B-doped sample)	Fig. 1b (Al-doped sample)	Fig. 1c (Cr-doped sample)
Dopant precursor	Boron powder	Trimethyl Aluminum $(CH_3)_3Al$	Bis(ethylbenzene) Chromium $(C_2H_5)_xC_6H_{6-x}$, x = 0-4
Laser (Nd:YAG laser, 1064 nm wavelength) operation mode	Continuous wave mode for 1st scan and pulsed mode (Q-switched, 5 kHz) for 2nd scan	Pulsed mode (Q-switched, 5 kHz)	Pulsed mode (Q-switched, 5 kHz)
Laser Power [W]	10.5 (1st scan), 12.5 (2nd scan)	10.5 – 11.2	12.5 - 13
Beam diameter at the focusing lens [mm]	2	2	2
Focal Length [mm]	150	150	150
Scanning Speed [mm/s]	0.8	0.8	0.8
Assist Gas	Argon at 30 psi	Argon at 30 psi	Argon at 30 psi
Position of the sample from the focusing lens [mm]	160-162 (1st scan), 140-135 (2nd scan)	140-142	140-144

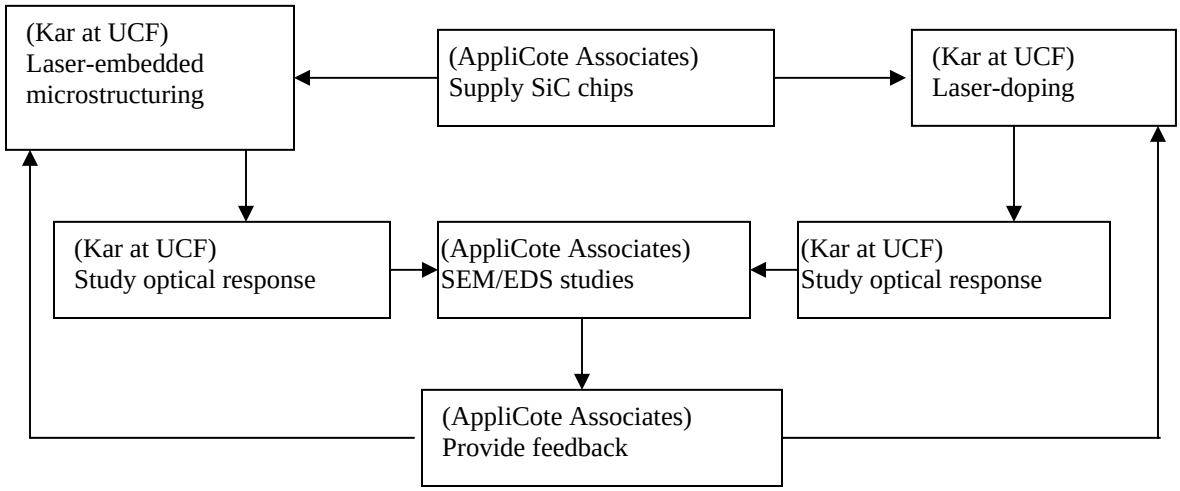

Figure 10. Project activities for SiC chip development, chip fabrication and optical response studies.

G.2 SiC Industrial Probe Design and Testing for High Temperatures and Pressures

Recently, Riza et.al. have proposed, designed, and demonstrated a new class of smart hybrid wireless-wired extreme environment temperature and pressure sensors using single crystal SiC optical chips and engineering optics and mechanics [5-6]. A critical aspect of these smart sensors is the packaging of the thick single crystal SiC optical chip within the appropriate front-end sensing assembly suited for temperature and/or pressure measurement. A particular application in fossil-fuel based power plants is extreme temperature measurement in the hot-gas combustion chambers. Fig. 11 shows an example proposed smart sensor system design suited for the required application that engages a long front-end probe that is inserted into the hot pressurized chamber. Temperature data taken off the chip in the probe represents the gas temperature and is read by a smart transceiver system with automatic alignment. Multi-wavelength signal processing using the retro-reflected optical power data produces the hot gas temperature.

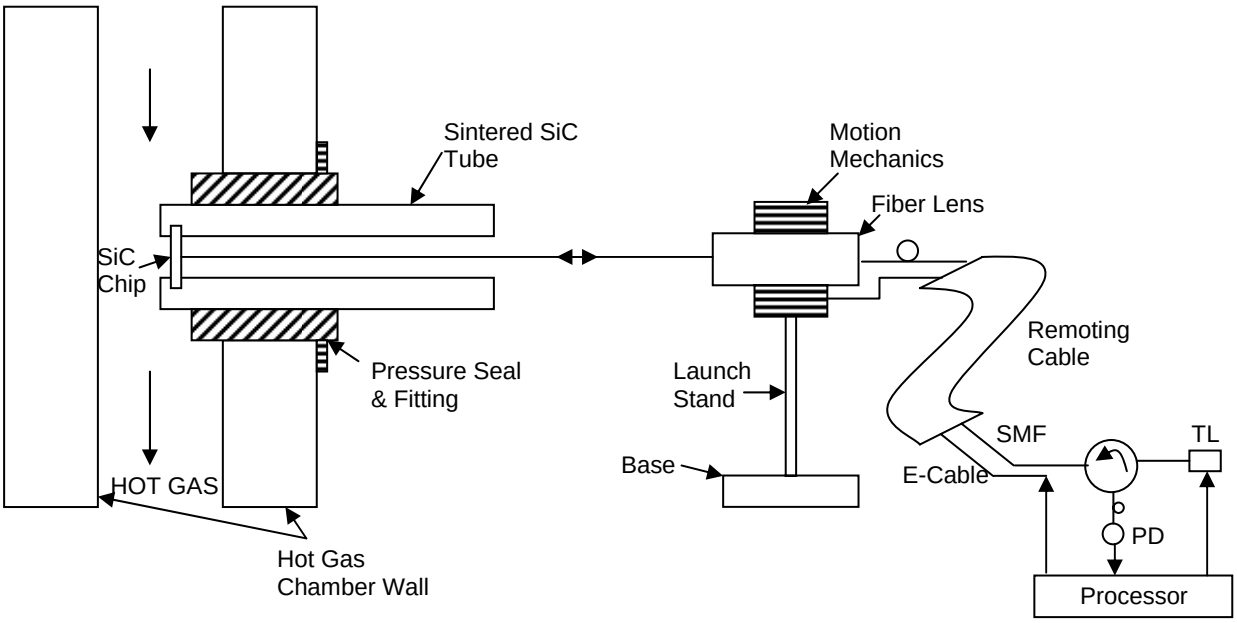

Fig. 11: Proposed Extreme Temperature Hybrid Design Optical Sensor using SiC sensing and packaging technology. PD: Photo-Detector; TL: Tunable Laser; SMF: Single Mode Fiber.

Fig.12 Example High Pressure High Temperature Seal SiC Tube that forms the basis of the SiC chip front-end packaging.

Fig.12 shows an example high pressure high temperature seal SiC tube that forms the basis of the SiC chip front-end packaging. The tube has ~ 17 inches long with 1.25 inch outer diameter and 0.75 inch inner diameter and cemented carbon steel bushing for pressure seal.

Fig. 13 shows the custom fabricated laser beam transceiver module which includes the high precision motion controller stage with the fiber lens mounted on it. This transceiver module has the capability of moving the laser beam $\pm 4.5^{o}$ in both the horizontal and the vertical directions as shown in Fig. 14 scenario under test. The transceiver mechanics is controlled by a computer and would be able to automatically align the system back into retro-reflective mode using the feedback from the photo-detector even if the probe moves because of vibrations in the

gas chamber. This smart design is critical to enable probe deployment in practical combustion chamber scenarios with vibrations.

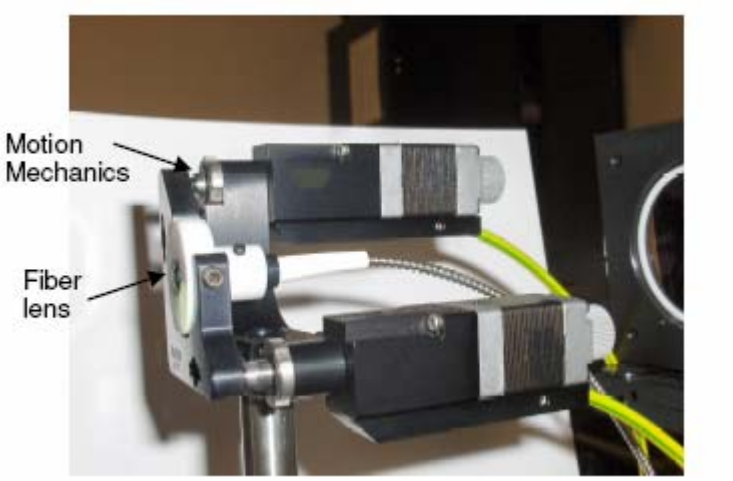

Fig. 13: Fabricated Laser Beam Smart Transceiver Module using Electronically Controlled Beam Alignment Mechanics.

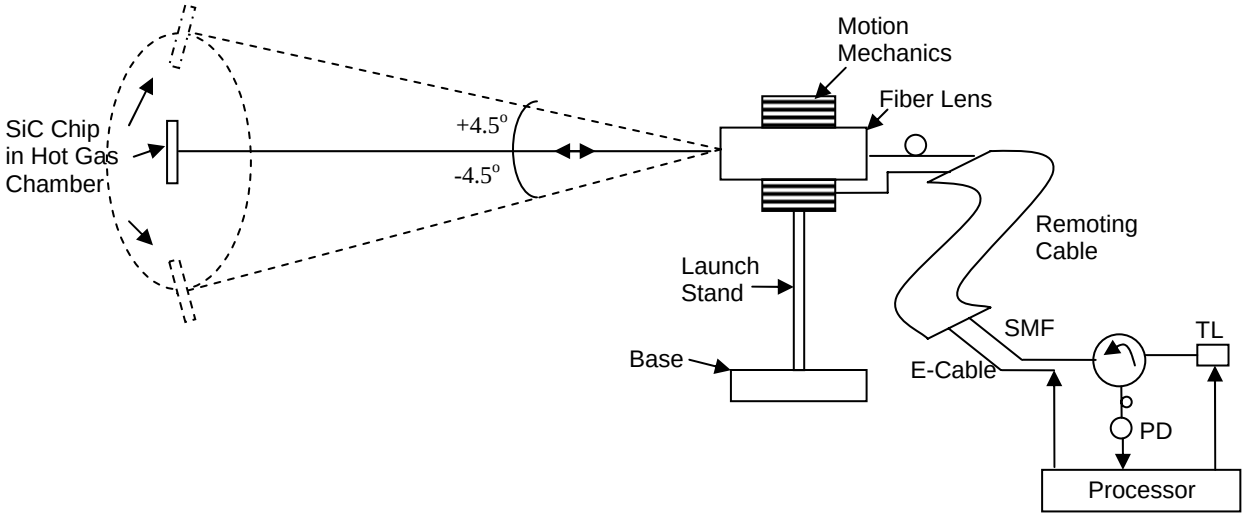

Fig. 14: Automatic system alignment scenario in case of movement of SiC chip in probe within hot gas chamber.

Fig. 5 (a) – (i) shows the conducted laser beam alignment and tracking tests. The laser beam coming out of the transceiver module in shown in various positions on a screen. These figures demonstrate the $\pm 4.5^{o}$ of movement of the laser beam over a distance of 60 cm from the fiber

lens as seen by an imaging camera. These results show the smart power of the proposed sensor system.

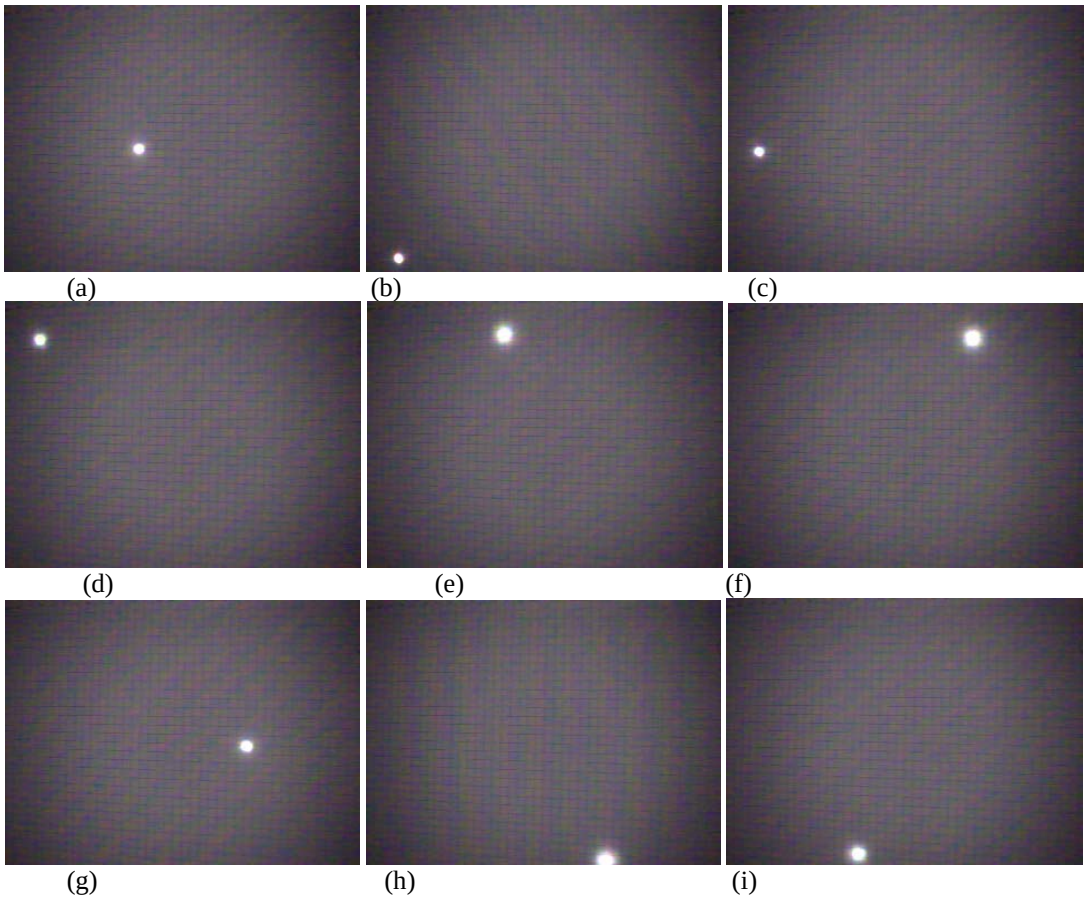

Fig. 15. Laser beam from the transceiver module in various positions on a screen.

H: RESULTS AND DISCUSSION

SiC Chip-based Gas Species Optical Sensing at High Temperatures and Pressure:

The Kar LAMP Lab. led conclusions is that the effects of a single gas (N_2) and combustion gas mixtures on the optical response of a silicon carbide chip has been studied as a function of temperature and pressure. The reflected power off the SiC chip exhibited unique interference patterns at high pressures and temperatures. These patterns have been utilized by Kar.et.al to determine the refractive index of a compressed layer at the chip-gas interface in order to show that the SiC chip can identify the combustion gases. The compressed layer refractive indices are different for different combustion gas species. The combustion gas such as hydrogen in nitrogen at a given temperature (T*) and pressure (P*) reduces the refractive index of compressed layer compare to pure nitrogen gas has been used for that same temperature (T*) and pressure (P*) whereas The combustion gas such as carbon monoxide, carbon dioxide, methane, etc., in nitrogen at a given temperature (T*) and pressure (P*) increases the refractive index of compressed layer compare to pure nitrogen gas has been used for that same temperature (T*) and pressure (P*). Kar LAMP Lab. conclusion is that this data can be used to detect different combustion gas species.

SiC Industrial Probe Design and Testing for High Temperatures and Pressures

A basic probe design has been implemented including the fabrication of probe components such as front-end packaging tube, smart transceiver optics, and smart motion mechanics. Experiments on the smart laser beam pointing and tracking have been conducted to yield positive results.

I: CONCLUSION

In conclusion, this report describes work that has evolved to meet the 2006 Oct. 1 to March 31, 2007 stated objectives of (a) fabricate specific embedded phase microstructured (or doped) SiC chips and evaluate use of SiC chip in remote optical sensing of individual gas species such as found in combustion chambers and (b) conduct temperature probe design, assembly and initial testing.

J: REFERENCES

[1] Atallah E. Batshon, Jonathan C. Backlund, Alternate Fuels for Supplementary Firing Add Value and Flexibility to Combined Cycle and Cogeneration Plants, Power-Gen International 2001, December 11-13, 2001.

[2] G. Cocurullo, F. G. Della Corte, I. Rendina, Temperature dependence of the thermo-optic coefficient in crystalline silicon between room temperature and 550 K at the wavelength of 1523 nm, Applied Physics Letter, V 74, No. 22, 1999, pp. 3338.

[3] S. Dakshinamurthy, N.R. Quick and A. Kar, SiC-based optical interferometry at high pressures and temperatures for pressure and chemical sensing, Journal of Applied Physics, Vol. 99, 2006, pp. 094902-1 to 094902-8.

[4] S. Dakshinamurthy, N.R. Quick and A. Kar, Temperature-dependent optical properties of silicon carbide for wireless temperature sensors, J. Phys. D: Appl. Phys., Vol. 40, 2007, pp. 353-360.

[5] N. A. Riza, M. A. Arain, and F. Perez, “Harsh Environments Minimally Invasive Optical Sensor using Freespace Targeted Single Crystal Silicon Carbide,” IEEE Sensors Journal, Vol. 6, No. 3., pp 672-685, June 2006.

[6] N. A. Riza, F. N. Ghauri, and F. Perez, “Wireless Pressure Sensor using Laser Targeting of Silicon Carbide,” Optical Engineering, Vol. 46, No. 1, pp 014401, Jan. 2007.